BAMS Article

Incorporation and Use of Earth Remote Sensing Imagery within the NOAA/NWS Damage Assessment Toolkit

Andrew L. Molthan, Lori A. Schultz, Kevin M. McGrath, Jason E. Burks, J. Parks Camp, Kelsey Angle, Jordan R. Bell, and Gary J. Jedlovec

ABSTRACT: Severe weather events including tornadoes, damaging winds, hail, and their combination produce changes in land surface vegetation and urban settings that are frequently observed through remote sensing. Capabilities continue to improve through a growing constellation of governmental and commercial assets, increasing the spatial resolution of visible, near to shortwave infrared, and thermal infrared remote sensing. Here, we highlight cases where visual interpretation of imagery benefitted severe weather damage assessments made within the NOAA/NWS Damage Assessment Toolkit. Examples demonstrate utility of imagery in assessing tracks and changes in remote areas where staffing limitations or access prevent a ground-based assessment.

https://doi.org/10.1175/BAMS-D-19-0097.1
Corresponding author: Andrew L. Molthan, andrew.molthan@nasa.gov
In final form 31 October 2019

AFFILIATIONS: Molthan and Jedlovec—Earth Science Branch, NASA Marshall Space Flight Center, Huntsville, Alabama; **Schultz and Bell**—Earth System Science Center, University of Alabama in Huntsville, Huntsville, Alabama; **McGrath and Burks**—Cooperative Institute for Research in the Atmosphere, Colorado State University, Fort Collins, Colorado; **Camp**—NOAA/National Weather Service/Weather Forecast Office, Tallahassee, Florida; **Angle**—NOAA/National Weather Service/Weather Forecast Office, Springfield, Missouri

Following a severe weather event, meteorologists in NOAA's National Weather Service (NWS) typically perform a detailed damage assessment if a tornado has been observed or suspected, complementing activities by emergency managers, affected citizens, insurance providers, and supporting organizations. Collection of damage assessment information includes collaborations with these groups during the event, site visits, rigorous data entry, and quality control to synthesize key details into the official NOAA/NWS Storm Data record. Timeliness is critical: assessments are performed as rapidly as possible to ensure documentation of known damage indicators prior to any cleanup. Assessments are relied upon by downstream users to map impact and recovery needs including efforts by local and state emergency managers, the Federal Emergency Management Agency (FEMA), insurance companies, and local governments (Edwards et al. 2013).

In 2005, work toward a streamlined approach to the damage assessment process was initiated by the NWS Weather Forecast Office (WFO) at Omaha/Valley, Nebraska. Efforts began with laptops, GIS software, and handheld GPS devices to expedite collection and mapping. In parallel, staff at WFO Shreveport, Louisiana, and Tallahassee, Florida, were using Blackberry devices to assist with damage assessments by establishing a prototype web interface to assist with collection and quality control of information (Pearson and Lander 2008; Stellman et al. 2009; Leonardo 2011). Through these efforts, a team was formed to develop and evolve these capabilities into the current NOAA/NWS Damage Assessment Toolkit (DAT). Using the DAT, NWS meteorologists and assessment participants collect damage information through geotagged photos and in-app questionnaires that tie observations to appropriate enhanced Fujita (EF)-scale damage indicators (National Wind Institute 2006). Collected assessment information is centralized by an Esri ArcGIS Server (now Esri Enterprise) and other Esri software tools. The DAT supports collaboration by allowing those in the field to collect information for corroboration with complementary datasets. For example, the DAT can incorporate Civil Air Patrol photography (CAP; when available) and weather radar observations to place observed damage within a meteorological context. Often, this is a team effort between field assessment teams, personnel on station at WFOs, and their Regional Operations Center. These collaborative efforts ensure quality control and consistency before their highest-quality assessment and supporting analyses are shared with the general public.

Development and early use of the DAT coincided with major severe weather events in 2011. The DAT was used to complete damage assessments within the Birmingham, Alabama, WFO coverage area for the 27 April 2011 tornado outbreak (Knupp et al. 2014; NOAA 2019b), the 22 May 2011 tornado in Joplin, Missouri (NOAA 2019e), and the Moore, Oklahoma, tornado of 2013 (Camp et al. 2014) where visibility of DAT usage and other outreach encouraged incremental adoption by several WFOs for local events. Today, NWS operations now includes the DAT as the mechanism for gathering storm damage assessment information (NOAA 2018).

Numerous tornado events are now available online as a growing event archive composed of detailed tracks and supporting damage indicators.

Application of remote sensing to identifying severe weather damage. Several studies have applied land surface remote sensing and change detection approaches to identify damage from winds, hail, and tornadoes. Yuan et al. (2002) used single-day normalized difference vegetation index (NDVI; Tucker 1979) scarring, principal components analysis, and NDVI change techniques to visualize and measure the rural and urban damage regions in the F2–F3 categories of the 3 May 1999 tornado in Oklahoma City, Oklahoma, and surrounding areas. Myint et al. (2008) examined tracks from the 3 May 1999 tornado in the Oklahoma City area using *Landsat-5* imagery, applying PCA across the six Thematic Mapper bands at 28.5 m spatial resolution with their algorithm scoring as high as 98% accuracy against specific F-scale values. Remote sensing and aerial imagery have been used in combination with available radar data to help diagnose tornadogenesis locations and relationships to convective structure (Skow and Cogil 2016).

Jedlovec et al. (2006) used the MODIS aboard NASA's *Terra* and *Aqua*, the NASA/JAXA ASTER aboard *Terra*, and the *Landsat-7* ETM+ to extract damaged areas resulting from the La Plata, Maryland, tornado of 28 April 2002 and other midwestern U.S. hail events. Molthan et al. (2014) used visual examination of single-day NDVI from ASTER (15 m), ETM+ (30 m), and MODIS (250 m) for identification of tornado tracks across Alabama following the 27 April 2011 tornado outbreak. Research expanded upon previous use of postevent ASTER and MODIS imagery with Alabama NWS partners in the immediate aftermath of the 27 April 2011 outbreak (Molthan et al. 2011). Lengths of visually identified damage correlated more favorably to the official damage assessment tracks than width (e.g., R^2 of 0.93 for *Landsat-7* ETM+ pathlengths vs 0.41 for widths), due in part to greater difficulty in capturing lower-end damage with distance away from the centerline of the assessed damage path. Kingfield and de Beurs (2017) developed a disturbance index (DI) from Landsat surface reflectance and comparisons of nondamaged pixels and an undisturbed background. They demonstrated benefits from using their DI approach over NDVI, which returned to cyclical, seasonal changes in greenness over time.

Additional studies have examined how remote sensing can provide mapping over a range of spatial scales, down to building-level information. Womble et al. (2018) describe ongoing work to apply multiple spatial scales (tiers) of remote sensing to the damage assessment process. In their tiered approach, Earth-observing satellite imagery have demonstrated application to mapping the broad damage path (Tier 1, e.g., Molthan et al. 2014; Jedlovec et al. 2006; Myint et al. 2008). Higher-resolution satellite and aerial imagery can provide more detailed structural damage assessment (Tier 2). Brown et al. (2012) developed quantitative methods to relate high-spatial-resolution imaging of structures to damage criteria in the EF scale. Currently, NWS meteorologists are focusing on observed damage indicators and their associated range of wind speeds, which are then linked to the intensity of the tornado at that specific location. Even higher-resolution imagery from low-altitude flights, drones, or specialized commercial imaging may also provide individual building assessment (Tier 3). Specialized 3D photography and laser or lidar scanning may provide structure-level details highlighting specific aspects of building engineering and design (Tier 4). These platforms may be available in high-impact events from CAP or specific deployments of imaging assets by supporting agencies and private-sector contractors.

The growing volume of satellite remote sensing and approaches motivated exploratory efforts to incorporate this information in the damage assessment process. To increase the amount of information available to support the damage assessment process, the NASA Applied Sciences Disasters Program awarded a feasibility study to integrate Earth remote sensing

Table 1. List of products incorporated into the Damage Assessment Toolkit for evaluation by NOAA/NWS partners. Asterisk indicates that EO-1 provided capabilities similar to Landsat and ended in March 2017.

Provider	Satellite	Sensor	Resolution	Repeat	Products
Near-real-time or routinely available products					
NASA	*Terra*	MODIS	250 m	Daily	True color and NDVI
		ASTER	15 m	Targeted	False color
	Aqua	MODIS	250 m	Daily	True color and NDVI
NOAA	*Suomi NPP*	VIIRS	375 m	Daily	True color and NDVI
USGS/NASA	*Landsat-8*	OLI	30 m	16 days	True/false color, NDVI
		OLI	15 m		Panchromatic
	Landsat-7	ETM+	30 m	16 days	True/false color, NDVI
		ETM+	15 m		Panchromatic
USGS/NASA	EO-1*	ALI	30 m	Targeted	True color, NDVI
Event-specific requests via USGS Hazards Data Distribution System					
DigitalGlobe	*Worldview-1/2/3*	Various	<5 m	Targeted	True color, false color, panchromatic
CNES	SPOT	Various	<6 m	Targeted	False color
Airbus	Pléiades	Various	<2 m	Targeted	True color
ESA	*Sentinel-2*	MSI	10–60 m	10 days	True color, NDVI, false color
Complementary radar information					
NOAA	Multi-Radar Multi-Sensor (MRMS) system	WSR-88D	Daily	0.01°	Maximum hail size, mesocyclone tracks

information in the DAT. By the time the project kicked off, a small number of NWS WFOs had already experimented with using satellite imagery in local desktop GIS systems. Experienced staff members from these offices, DAT developers, the feasibility study team, and other NWS collaborators met in two annual meetings to establish collaboration goals focused on DAT usage and improvements. Outcomes focused on partnerships with NWS WFOs in central and southern region who were increasing their adoption of the DAT for local damage assessments, who had experience with CAP and remote sensing imagery, and who would provide feedback on the benefits of including remote sensing imagery within the DAT client. Herein, we report on these collaborative efforts and include a subset of cases where partners demonstrated the value of imagery in the assessment process. Outcomes here focus on the following:

- Documenting platforms providing visible and near-infrared imaging or derived parameters (e.g., derived indices, false color composites) that were made available to the DAT to qualitatively assess their value in visual interpretation during the damage assessment process
- Describing use case examples that qualitatively and quantitatively demonstrated improvements in severe weather damage assessment efforts through application of Earth remote sensing data

Incorporation of remote sensing in the Damage Assessment Toolkit

Remote sensing imagery from a variety of platforms were provided to damage assessment teams to determine their effectiveness for qualitative interpretation supporting damage track assessment and adjustment (Table 1). Based upon past demonstrations of track identification from polar-orbiting missions offering daily coverage (Molthan et al. 2014), NASA's *Terra* and *Aqua* MODIS and the NASA/NOAA *Suomi NPP* VIIRS imagery were used to generate daily NDVI and true color composites. True color, false color, NDVI, and higher-spatial-resolution panchromatic imagery from *Landsat-7* ETM+ were made available in early phases of the project and then replaced by comparable *Landsat-8* OLI imaging, alleviating issues with missing *Landsat-7* ETM+ pixels due to the scan-line corrector failure. Repeat coverage was provided

every 16 days. For major events, USGS and NASA collaborate with JPL for tasking of *Terra*/ASTER to contribute 15 m NDVI and false color composites for damage swaths targeted within view of the *Terra* ground track.

To complement routine imaging, event-specific requests were often made to the USGS Hazards Data Distribution System (HDDS). Meteorologists at WFOs provided areas of interest in collaboration with their Regional Operations Center through use of the USGS/HDDS Collection Management Tool (CMT). As imagery for the target area became available, they were loaded into HDDS and made available for download. Eagle Vision teams within the Department of Defense collaborate with USGS HDDS to provide collections from the French commercial Système Pour l'Observation de la Terre (SPOT; translated System for Observation of Earth) series. SPOT provides visible and infrared bands comparable to *Terra* ASTER and *Landsat-7*/*8*, over a smaller coverage area but at higher spatial resolution than Landsat.

Through the NextView data and license agreement, USGS HDDS frequently acquires DigitalGlobe *Worldview-1*, *Worldview-2*, and *Worldview-3* visible and near-infrared imagery (~1 to 5 m) and a separate panchromatic band (0.3–0.46 m, sensor specific). Beginning in 2018, USGS HDDS also provided a pan-sharpened version that combines the best of the visible, near-infrared, and panchromatic into a single image (*Worldview-3* only). Planet Labs has recently begun contributing their imagery to response for major disaster events and may serve as an additional imaging resource for future response efforts. Due to the NextView licensing agreement, distribution and use of some products is limited to disaster response activities. The DAT includes flags to advise NWS staff on their need for limited distribution to state and federal partners involved in disaster assessment and recovery operations.

Other imaging assets are occasionally provided for large U.S. events affecting multiple states through activation of the International Charter on Space and Major Disasters (https://disasterscharter.org). These have included multistate tornado outbreaks, landfalling hurricanes, and regional flood events. When activated, the Charter is supported by a project manager who coordinates international partners in acquiring and providing imagery from which additional products can be derived. For example, Pléiades imagery from Airbus Defense and Space are a frequent contribution, including 0.5 m imaging following the 20 May 2013 tornado in Moore and 28 May 2019 event near Lawrence, Kansas (not shown). For inclusion in NWS/DAT efforts, Charter products are nonautomated and event-specific, often requiring additional days to collect cloud-free views subject to satellite orbit considerations.

Combined, free and open datasets from domestic and international sources and those from a growing set of limited access, private sector platforms offer substantial imaging capabilities during major disaster response scenarios. In parallel, many private companies offering satellite imaging are releasing their imagery to the general public through their own web pages, social, and traditional media outlets.

For test and evaluation purposes of imagery within the DAT, automated scripts acquired imagery via HDDS and other NASA sources. Imagery was postprocessed to top-of-atmosphere reflectance in various channels from the visible to near-infrared and provided for analysis. To incorporate imagery within the DAT, products were placed on a local web mapping service (WMS), using the Java-based Geoserver and GeoWebcache to support image caching and improved performance. In addition, a RESTful web interface was created to support data ingest and purge (45-day retention), along with an interface to pull imagery for analysis based upon the geographic area of interest and event times reported from the DAT software. Products requiring a specific legend or color map were provided with a visualized legend to aid in color interpretation. A summary of technical components and their relationships is shown in Fig. 1. At the request of NOAA/NWS WFOs and regional partners, processing and delivery includes Multi-Radar Multi-Sensor (MRMS) system 24-h composites of rotation tracks and the maximum estimated size of hail (MESH), each ending at the time nearest 1200 UTC of

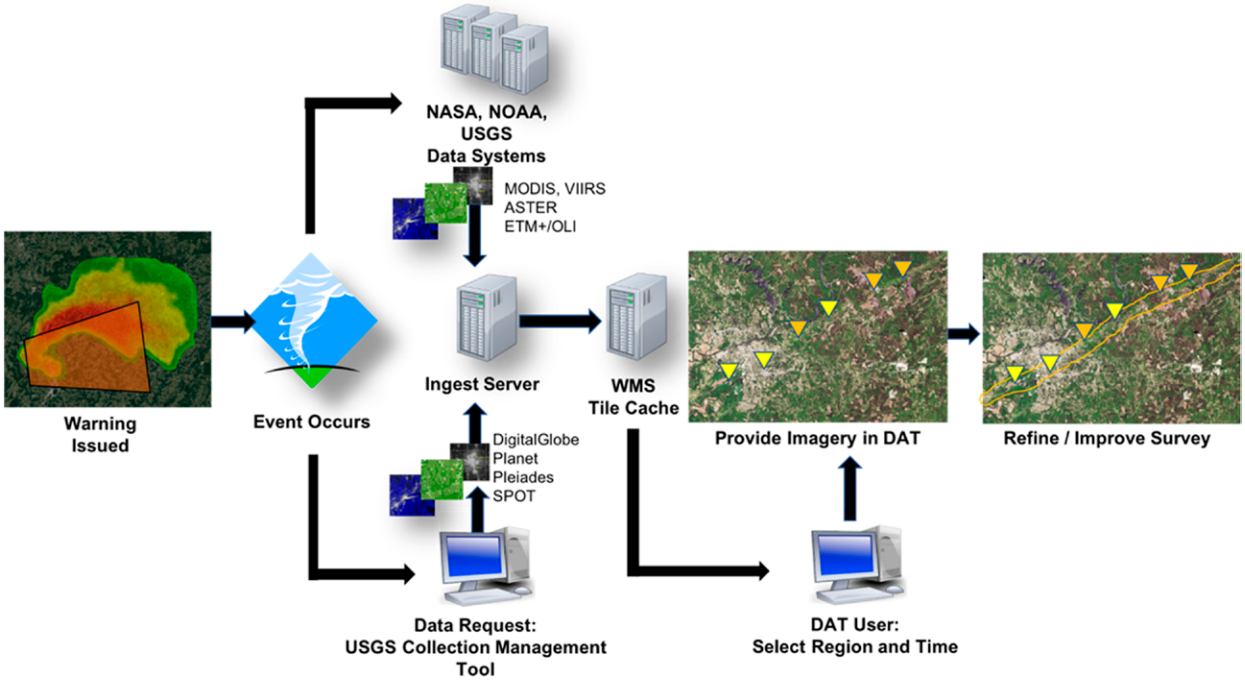

Fig. 1. An overview of data request, integration, and dissemination processes for inclusion of remote sensing information within the DAT for purposes of evaluation and demonstration. Survey shown is hypothetical and for demonstration purposes.

each day. These fields were requested for visual comparison of radar information to ground assessment details and potential signals observed in satellite imagery.

Training materials for data access and visual interpretation. The development team provided training material through informal and formal methods to improve access to, and utilization of, remote sensing imagery within the damage assessment process. Topics included 1) processes for submitting a specific data request via USGS CMT, 2) accessing routine and event-specific products made available through the DAT, and 3) specific strengths, weaknesses, and interpretation guidance for various products based upon experiences of the development team and partnering NWS field meteorologists. Developers created brief YouTube videos shared during regional webinars and with NWS field office partners testing the application of remote sensing imagery within the storm damage assessment process (Camp 2013a,b). These videos and webinars focused on explaining the various sources of remotely sensed imagery, the process of requesting supplemental higher-resolution imagery in collaboration with USGS HDDS, and other procedural steps requiring assistance from either NWS Regional Operations Center staff or others within their local office. As the project developed, these informal webinars were further expanded into online modules. The modules are now included as part of a broader storm damage assessment and DAT tutorial served by the Department of Commerce Learning Management System and available online for the general public (NOAA 2019a).

While methods to objectively extract information on damage regions continue to be developed for individual sensors (Kingfield and de Beurs 2017; Molthan et al. 2013, 2014), resources available through HDDS, the International Charter, and other external sources are diverse and vary between events. To ensure the broadest possible use of a growing portfolio of imagery from the constellation of available satellites, training and usage focused on visual interpretation of imagery in the context of available public storm reports and radar data. The diversity of available imagery and emphasis on visual interpretation led to creation of online modules to describe data access and supplemental 1–2 page Quick Guide PDF documentation for the most common types of imagery products [Short-term Prediction Research and Transition Center

(SPoRT); NASA SPoRT 2019]. Each included an example of the products available from a given platform and sensor, information on the typical repeat cycle and latency, spatial and spectral resolution, and a brief list of the relative strengths and weaknesses of applying the imagery to storm damage investigations (Fig. 2). Materials were intended as complements to other DAT and operational training for current satellite missions. The design of training material was intentionally similar to others developed collaboratively with NWS meteorologists working with NASA SPoRT (Jedlovec 2013).

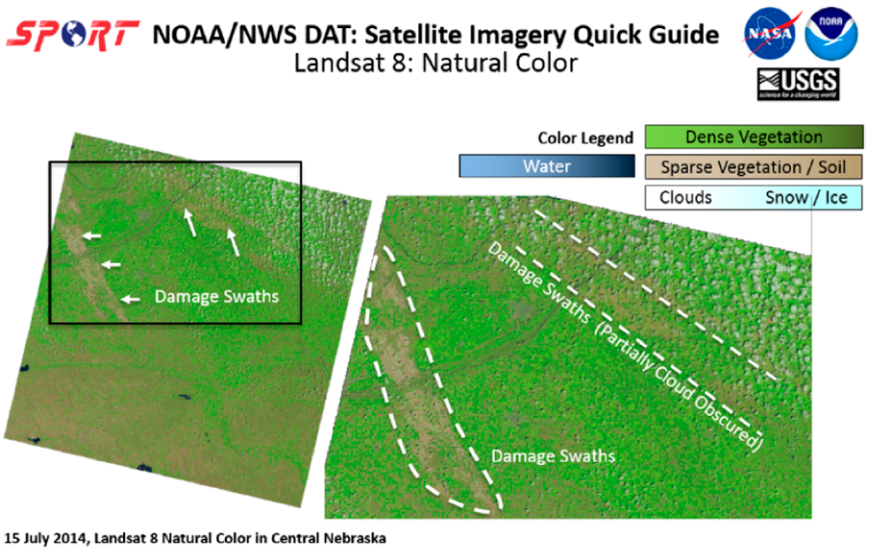

Access	SPoRT > Landsat 8 > Natural Color
Restrictions	None
Resolution	30 m
Latency	Landsat 8 has a 16 day repeat cycle. It observes the same location every 16 days.
Provider	USGS / NASA SPoRT
Spectral Bands	Three red and near-infrared bands (6,5,4) are combined to create an image similar to true color, but with additional discrimination of clouds and snow.
Application	Damage tracks are typically identified as brown scars against a green, vegetated background. Corroborate suspected damage tracks with other information.

How is the image generated?
- Reflectance in the red and near-infrared bands (6,5,4) is combined into a single false-color image to approximate a true color appearance.

What should I be looking for in this product?
- Red and near-infrared bands are often used to measure vegetation health. Tracks are apparent as linear features along the storm path, typically in shades of brown where vegetation and soils have been disrupted.
- Suspected track location can be corroborated with radar rotational track information or survey information.

What are the product limitations?
- Limited swath width may truncate portions of the track that continue outside of the scene.
- Clouds and cloud shadows may obscure portions of the damage track.

Fig. 2. An example of brief Quick Guide materials developed to support interpretation and use of imagery within the Damage Assessment Toolkit, shown here for *Landsat-8*.

Case studies

We highlight cases showing how NWS collaborators applied the use of the DAT and land surface imagery to improve characteristics of complex damage assessments. Our original intent and design was to provide immediate postevent imagery for use in the field, but latency in the request, collection, and posting of imagery led to more common use through in-office evaluation using the DAT web client. Assessment revisions were done through visual interpretation of true or panchromatic imaging for comparison to ground assessments, public reports, and available radar data. Through multiple events, partners tended to find greater levels of detail in higher-resolution commercial imagery when adjusting small-scale details of damage tracks, while coarser-resolution imagery still proved helpful in cases with long-track events leaving significant and long-term change.

Central U.S. tornadoes of 10–11 May 2015. On the evening of 10 May 2015, severe thunderstorms developed ahead of a cold front and area of low pressure in South Dakota (NOAA 2019c). As storms progressed to the northeast, interactions with a warm front led to tornadoes in Sioux and Calhoun Counties in west-central Iowa. Other public reports in Calhoun County included severe hail up to 2.75 in. diameter while storms in adjacent counties produced reports of damaging winds. Here, the damage assessment of interest focused on an EF-1 maximum intensity tornado that tracked near the communities of Lidderdale, Lake City, and Rockwell City, Iowa (Fig. 3).

DigitalGlobe Worldview and CNES SPOT imagery were made available in both true color and grayscale panchromatic. Though imagery from *Landsat-7* ETM+ became available on 14 May, the loss of the scan line corrector several years earlier meant too many pixels were missing for the imagery to be helpful. *Landsat-8* OLI complemented the ETM+ collection with observations on 17 May.

DigitalGlobe Worldview and CNES SPOT imagery were used by staff in the Des Moines, Iowa, forecast office to make a key correction in the overall length and direction of the tornado track, and to discriminate between areas of tornado damage and those likely caused by strong, straight-line winds associated with the supercell rear-flank downdraft. Prior to examining the imagery, damage assessors had developed a preliminary track to include damage indicators that began near Lidderdale and extended northeastward toward Lake City. Assessors noted that damage indicators near Lidderdale may not have been associated with the tornado damage path, and that additional investigation with radar would be required. When SPOT imagery became available on 12 May, the panchromatic imagery captured distinct swirl textures associated with scouring of an open field by the tornadic circulation but located to the north and west of the original damage assessment track. In combination with an examination of radar data, imagery guided the extension of the assessment polygon and track line southwest of Lake City into rural areas including those where field scarring was evident in SPOT imagery. As a result, the damage assessment team adjusted the tornado damage path to shift 4 km westward, adding about 1 km of length to the entire track, then separated this tornado track from damage indicators in the Lidderdale area that were instead attributed to damaging winds associated with the tornado-producing supercell (Fig. 3, pink shading).

Further examination of the SPOT imagery documented another brief tornado southwest of the city of Manson, Iowa (north of Lake City, not shown), which had also been reported by a severe weather spotter. Feedback from meteorologist Kevin Skow (then of WFO Des Moines and now WFO Topeka, Kansas) noted that "the modifications you are seeing in the DAT are a direct result of what we found in the satellite data. A second storm produced wind damage within a few miles of the actual tornado path that same night. The damage assessment team thought that this damage might be from the tornado. However, the satellite data showed that the path was farther to the northwest. The satellite data also helped us fine tune the path north of Lake City. The satellite data has proven once again to be a great asset for our storm surveying operations."

Farther north and west, collected imagery was also used by staff in WFO Sioux Falls, South Dakota, to verify the location of a damage track and to confirm information completed in their earlier damage assessment. Panchromatic imagery from *SPOT-6* was used to confirm track information particularly in rural areas where access was restricted, based upon observations of field scour and other features that could be visually interpreted (not shown).

Northern Illinois, southern Iowa, and central Michigan tornadoes of 22 June 2015. On 22 June 2015, supercell thunderstorms developed across the upper Mississippi Valley and Great Lakes regions, resulting in numerous wind and tornado damage reports in Iowa, southern Wisconsin, northern Illinois, and Michigan, and additional damaging wind reports farther east as the system progressed (NOAA 2019c). The WFO in Des Moines requested supplemental imagery through USGS HDDS to support damage assessments for tornadoes reported in the southern portion of their county warning area (CWA) for locations near Columbia and Albia, Iowa, and to the east of those communities near Eddyville, Iowa (not shown).

DigitalGlobe *Worldview-2* provided a first glimpse at areas of interest to the staff in Des Moines after acquiring imagery on 3 July, including multispectral and panchromatic views. Coverage of the DigitalGlobe scenes included the entire length of the previously assessed damage indicators for the tornado of interest (Fig. 4). In this scenario, satellite imagery helped

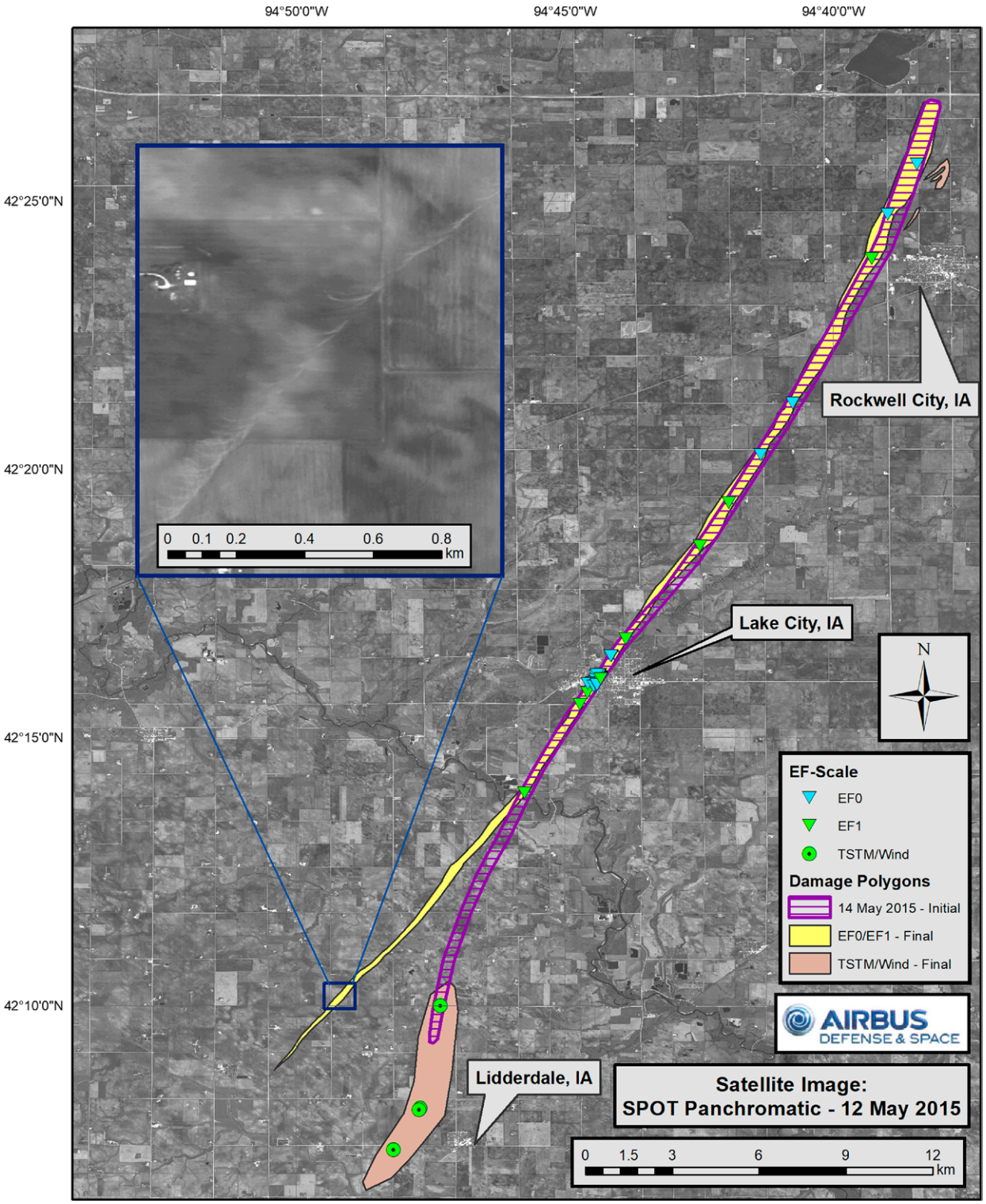

Fig. 3. Damage assessment polygons prior to (purple, hatched) and following (yellow and red, filled) the inclusion of 12 May 2015 SPOT imagery for analysis. Inset area is representative of field scarring from the tornado seen elsewhere in the SPOT image. The red shaded region and thunderstorm damaging wind indicators represent the area reassessed and classified following SPOT imagery analysis. Source imagery copyright 2015 through the NextView license.

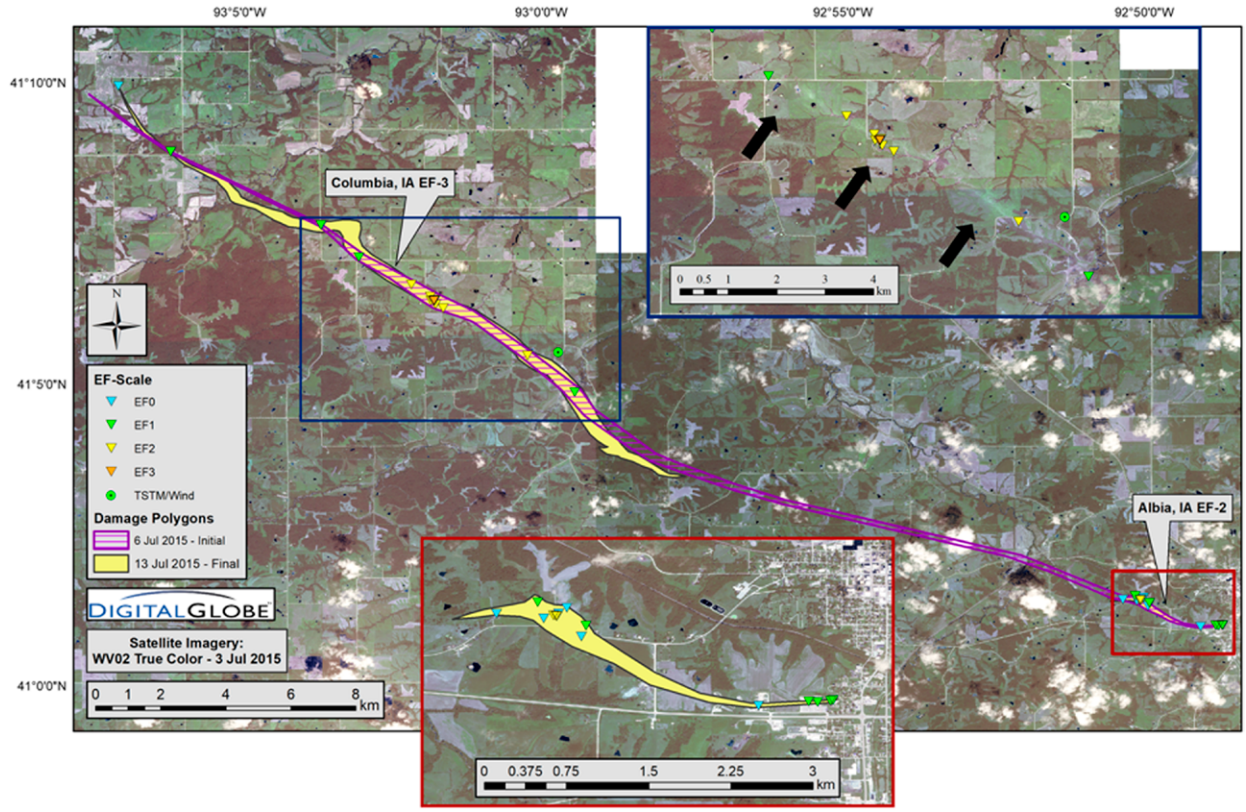

Fig. 4. As in Fig. 3, but for assessment of tornadoes in central Iowa from 22 Jun 2015. The original damage assessment (purple, hatched) was reassessed as two separate tracks through visual inspection of available DigitalGlobe imagery. Source imagery copyright 2015 through the NextView license.

to evaluate and quality control the original damage assessment and helped to investigate less-populated areas where access was restricted. Comments from the team documented how the imagery was used to separate the original, single track into two distinct tornado events:

Assessment partner and NWS meteorologist Kevin Skow stated for their team that "we've completed our analysis of the satellite data for the Columbia tornadoes and the Eddyville tornado. As usual, the satellite data proved of great help ...(and indicated) a break in the Columbia track, which we were unable to confirm on the ground assessment due to the poor road network and thus had originally kept it as one track. The satellite data also shows some interesting characteristics of the tornado, including a pivot point just prior to the tornado's intensification to EF-3, and concentrated areas of damage in valleys where there is an enhanced inflow into the tornado along the valley channel (seen before with other tornadoes). Due to the trees/grassland nature of the area, the true color imagery was more useful ...since the resolution was not quite high enough to discern downed trees but could pick out the color differences between the live and dead vegetation (basically, a rudimentary version of an NDVI comparison)."

The original assessment included a single tornado track assessed from south of Columbia to Albia for a distance of approximately 30 km (18.6 mi). A second track was located just to the east and south of Eddyville. Imagery from DigitalGlobe was used within the web-based DAT interface to further evaluate damage and revise the track. In this case, imagery provided spatial detail that was helpful for separating the original long-track tornado into separate tracks of varying impacts and maximum intensity. The EF-3 track through Columbia was reduced to approximately 18 km (11.2 mi) and separated from the additional track through Albia at a length of around 3 km (1.86 mi).

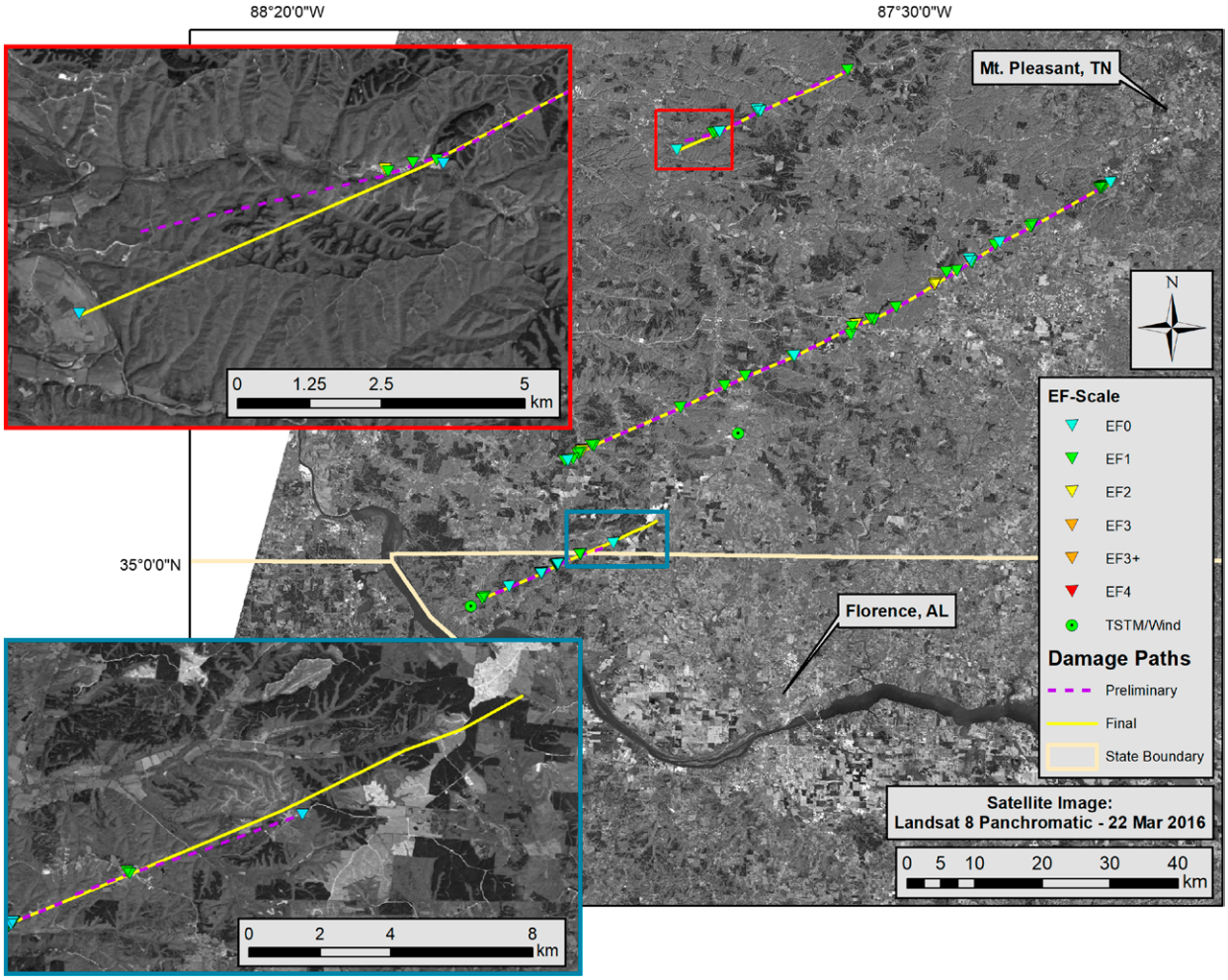

Fig. 5. Damage assessment tracks performed immediately following the 23 Dec 2015 severe weather events (purple) and final tracks as adjusted for two tornado events with tracks evident in *Landsat-8* imagery acquired on 22 Mar 2016.

The WFO in Grand Rapids, Michigan, also requested imagery supporting a damage assessment near Portland, Michigan. Imagery provided to the WFO was used to compare to available CAP photography. While satellite imagery was not specifically used to adjust their assessed track, users commented that the satellite perspective would be valuable for other events where CAP imagery was not widely available.

Middle Tennessee tornadoes on 23 December 2015. The evening of 23 December 2015 brought an unusual winter season tornado outbreak across Ohio and the Tennessee Valley. Many of the storms in northern Mississippi and western Tennessee led to long-track tornadoes, injuries, and fatalities. Here, we focused on tornadoes impacting the CWA of WFO Nashville, Tennessee (NOAA 2019d). Affected areas in middle Tennessee were primarily rural and largely inaccessible to the assessment teams, limiting observations of damage indicators, beginning, and end points.

Observations from *Landsat-8* captured several areas where the storm damage assessment teams could not otherwise obtain access, though occurring several months postevent (22 March 2016; Fig. 5). Given the alignment of the *Landsat-8* tracks to the storm tracks in late December and confirmation that the same signatures were not present preevent, feedback from partners at WFO Nashville stated "Landsat 8 imagery allowed NWS Nashville personnel to extend two of their tornado damage paths by several more miles than originally estimated" (Shamburger 2016). Two original tracks of 17 km (10.6 mi) and 22 km (13.8 mi) were each

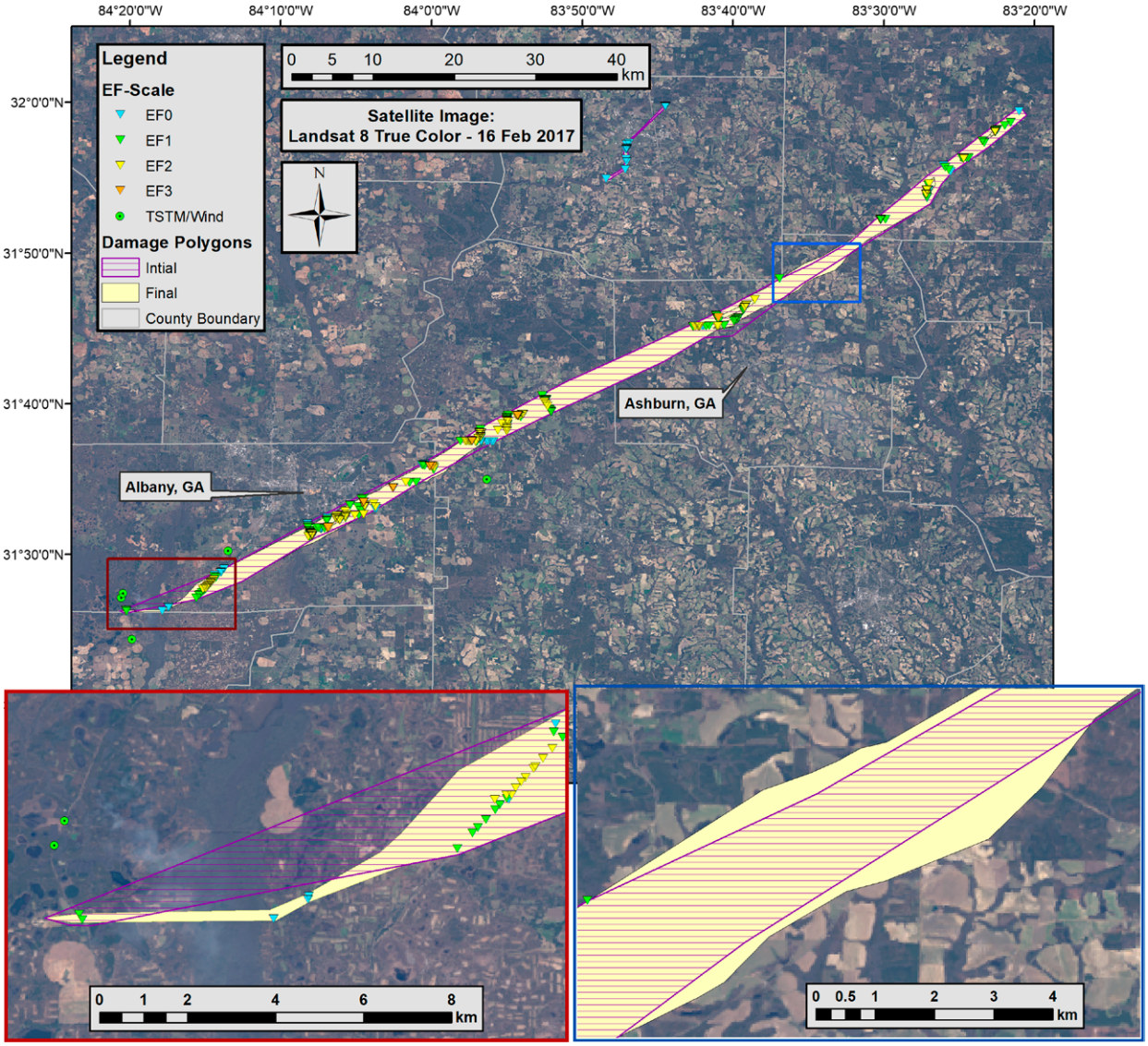

Fig. 6. As in Fig. 3, but representing analysis for the Albany long-track tornado from January 2017. Insets capture the southwestern portion of the track trimmed through imagery analysis (red), while the northeastern inset provides coverage for the coarse-resolution perspective of Fig. 7. Note that *Landsat-8* imagery is shown here as a base-map layer.

extended to total lengths of approximately 24 km (15 mi) using Landsat to map their extent through areas otherwise inaccessible during the original damage assessment process.

South Georgia tornadoes of 22 January 2017. An EF-3 tornado occurring in an SPC high-risk area traveled along a pathlength of 114 km (70.8 mi), impacting Albany, Georgia, and points farther to the northeast, sustained by the northward propagation of an advancing warm front (NOAA/NWS 2019f).

DigitalGlobe and SPOT imagery were received by WFO Tallahassee to supplement their detailed ground damage assessment process. Products were used to refine the outer perimeter of inferred EF-0 categorical damage and make other adjustments to interior damage polygons (Fig. 6). In the southwesternmost portion and origin of the track, the initial damage assessment was extrapolated southwestward from a detailed series of damage indicators acquired along an available roadway. When DigitalGlobe imagery became available after the damage assessment, visual inspection lacked indications of downed trees, scattered debris, and other features present throughout regions of the original damage area. Inference from the satellite imagery was used to trim the damage polygon to 0.25 km in width from the original ~1.5 km

over a distance of ~6 km, constrained to connect ground-based damage assessment points composed of EF-0 to EF-1 categorical damage.

Farther to the northeast, just beyond the community of Ashburn, Georgia, damage assessment teams were limited in their ability to collect damage photos and indicators. However, imagery from DigitalGlobe revealed downed trees (purple inset, Fig. 7) outside the northern edge of the original assessment polygon. On the southern side, imagery revealed additional downed trees and exposed, upturned root balls and fallen trees directed north or northeastward toward the passing storm and winds believed to be associated with the tornado circulation (yellow inset, Fig. 7). The outermost EF-0 intensity polygon was expanded in width by approximately 1 km, helping to capture greater detail in regions that were not immediately available from the damage assessment. In addition, the extensive length of the Albany tornado track would have been otherwise time prohibitive to map in full detail given limitations on staffing and access to areas where downed trees were present.

Summary and future work

Developmental activities to include Earth remote sensing imagery within the NOAA/NWS Damage Assessment Toolkit have led to the use of imagery from NASA, NOAA, international, and commercial providers in support of the severe weather damage assessment process. These activities were motivated by cases demonstrating the value of remote sensing in the mapping of severe weather impacts, and preliminary efforts by NWS WFO partners to use NextView licensed and other supporting imagery in assessment efforts.

Engagement with NWS meteorologists and storm damage assessment teams demonstrated value in refining damage assessments through the interpretation of true color and panchromatic imagery while other false color composites and derived indices (e.g., NDVI) were used for other events (not shown). Many uses of satellite imagery focused on identification of tracks in regions that would be difficult to otherwise access, due to limited road networks, travel distance, and other factors. Imagery supported assessment efforts by helping map damage perimeters and discontinuities, particularly in areas of poor accessibility. While a subset of supported events was discussed in detail, these capabilities have supported NWS WFOs and collaborative partners in their response to a growing number of severe weather events including floods and hurricanes (Fig. 8).

As the remote sensing community continues to develop objective measures of storm-specific change detection, the NOAA/NWS DAT can be leveraged to incorporate those products in the damage assessment process. For example, change detection approaches incorporating a more rigorous disturbance index could automate some detections as a complement to visual interpretation or true color imagery or NDVI (Kingfield and de Beurs 2017). Incorporation of automated change detection methods may prove most beneficial for lower-resolution sensors: algorithms detecting change at lower spatial resolutions may draw out details missed by subjective evaluation that are more apparent with higher-spatial-resolution data.

Remote sensing may encourage more routine mapping of hail damage for large events that occur during the peak of the growing season. Hail damage is frequently observed from geostationary (Klimowski et al. 1998) and polar-orbiting satellite imagery (Bentley et al. 2002; Parker et al. 2005; Gallo et al. 2012; Molthan et al. 2013) including efforts to automate these detections using information from the visible, near-infrared, and thermal infrared wavelengths (Bell and Molthan 2016). Gallo et al. (2019) used a large number of DAT-acquired crop damage photos to create damage categories and relate them to observed NDVI change. These remote sensing studies and preliminary efforts to corroborate remote sensing to crop damage may facilitate mapping of long-track swaths of hail damage inferred from various radar products (e.g., MESH; Witt et al. 1998; Stumpf et al. 2004; Lakshmanan et al. 2007).

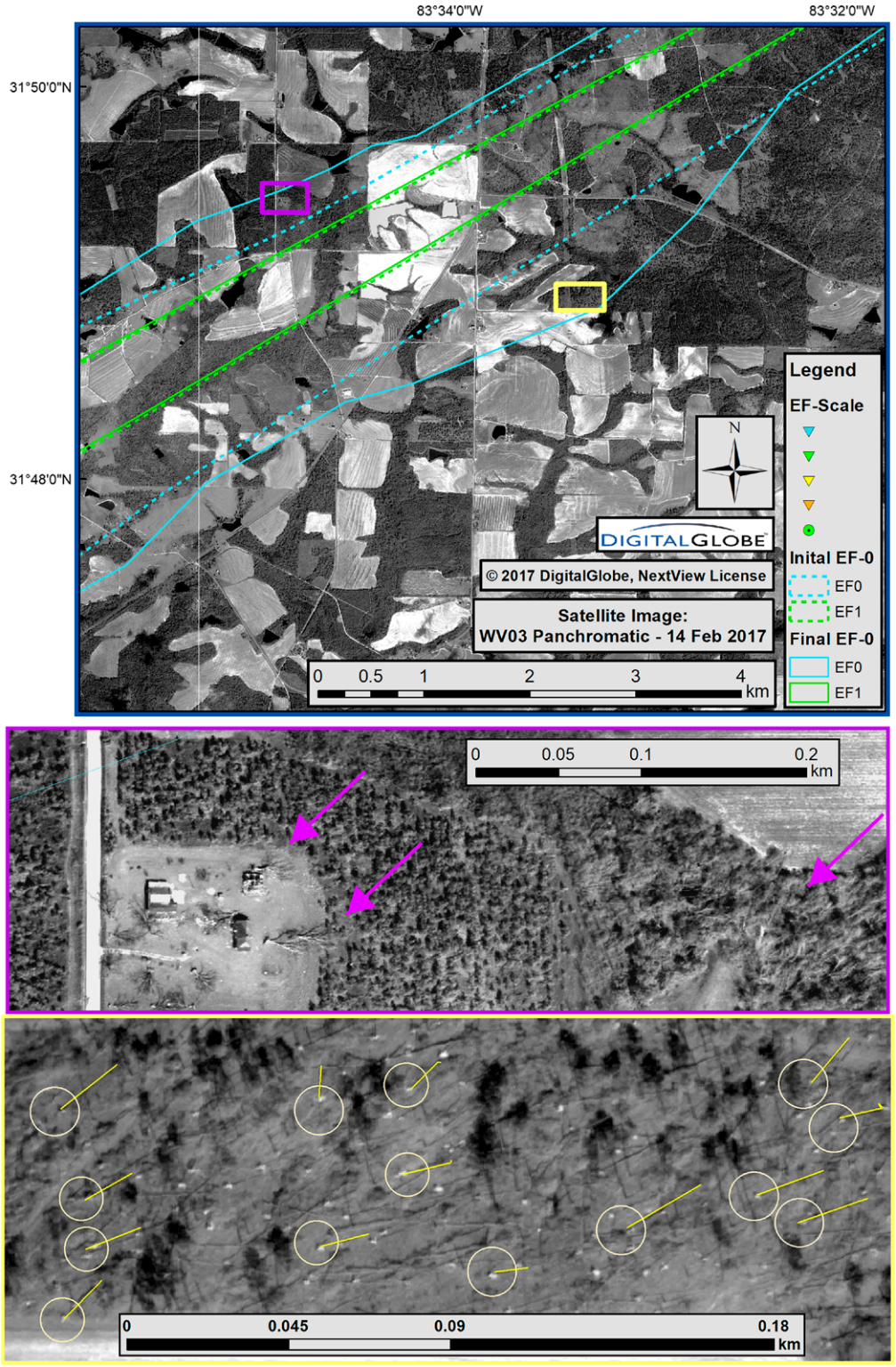

Fig. 7. (top) Zoomed inset of the northeastern portion of the Albany tornado track shown in Fig. 6 (blue box), along with additional insets capturing (purple) tree and structural damage to the northwest of the original EF-0 damage assessment polygon, and (yellow) inset identifying a region of downed trees (yellow lines) and associated upturned and exposed root balls as bright white features (yellow circles). Imagery shown here at reduced zoom factor to accommodate coverage area. Source imagery copyright 2017 through the NextView license.

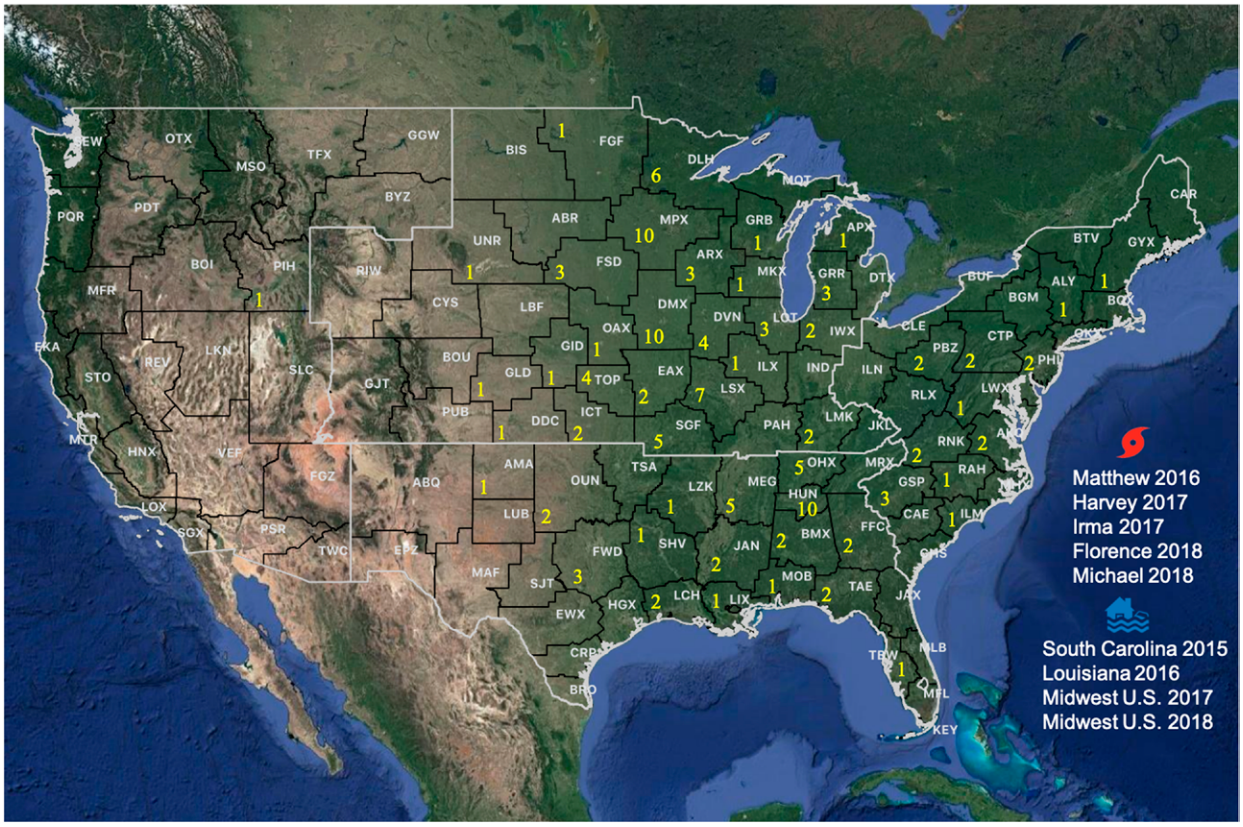

Fig. 8. Summary map of the continental United States, broken down by NWS WFO coverage area and number of events where USGS/HDDS support for tornado events was requested using the USGS/HDDS Collection Management Tool. In addition, major hurricane and flooding events were supported through USGS/HDDS collaborations and available imagery.

While clouds have proven challenging to the use of visible, near-infrared, and thermal remote sensing, free and open synthetic aperture radar (SAR) data [e.g., European Space Agency (ESA) *Sentinel-1A/B*] has demonstrated potential for the identification of tornado tracks (Schultz 2017) and hail damage (Bell et al. 2020) at C-band wavelengths. Free and open access to L- and S-band SAR is expected from the NASA–Indian Space Research Organization (ISRO) SAR Mission (NISAR; Rosen et al. 2015). SAR is advantageous because of its sensitivity to vegetation structure, nighttime imaging, and many platforms operating at wavelengths penetrating all but the heaviest of rain or snowfall rates.

Combinations of remote sensing and damage information may also benefit analysis of impacts from other hazards given available algorithms for mapping flood from polar-orbiting and geostationary satellites (Sun et al. 2012), burn scars (Giglio et al. 2009), and other damaging phenomena. The ever-expanding constellation of Earth remote sensing platforms from NASA, NOAA, international, and commercial sources continues to provide new capabilities with a growing number of spectral bands, higher spatial resolution, and reduced data latency. We hope that these advancements and continued inclusion of imagery will motivate new automated techniques and broader use of imagery within the damage assessment process with potential to support emergency managers through mapping of additional disaster impacts.

Acknowledgments. Developmental activities to include Earth remote sensing in the NOAA/NWS DAT were sponsored through grants to NASA Marshall Space Flight Center via the NASA Applied Sciences Disasters Program (NNH11ZDA001N). The authors thank the USGS/HDDS for extensive collaborations spanning multiple years, disaster events, and scenarios, including collaborations with Brenda Jones (ret.), Rynn Lamb, and Brenda Ellis. The authors would also like to thank supportive collaborators within the NWS including (alphabetically) John Ferree (ret.), Paul Kirkwood, Jim LaDue, Sam

Shamburger, Kevin Skow, Thomas (TJ) Turnage, Keith Stellman, and Brittney Whitehead. The authors would also like to thank three anonymous reviewers and their supporting editor for helpful comments that improved the clarity and focus of this manuscript. Commercial imagery made available through collaboration with USGS/HDDS and the NextView license are shown here highlighting disaster response applications, and their use and supporting commentary does not represent a specific endorsement of a private sector entity or commercial solution by NASA, NOAA, or other author affiliations.

References

Bell, J. R., and A. L. Molthan, 2016: Evaluation of approaches to identifying hail damage to crop vegetation using satellite imagery. *J. Oper. Meteor.*, **4**, 142–159, https://doi.org/10.15191/nwajom.2016.0411.

——, E. Gebremichael, A. L. Molthan, S. Shrestha, L. A. Schultz, K. C. Payne, C. R. Hain, and F. J. Meyer, 2020: Complementing optical remote sensing with synthetic aperture radar observations of hail damage swaths to agricultural crops in the central United States. *J. Appl. Meteor. Climatol.*, https://doi.org/10.1175/JAMC-D-19-0124.1, in press.

Bentley, M. L., T. L. Mote, and P. Thebpanya, 2002: Using Landsat to identify thunderstorm damage in agricultural regions. *Bull. Amer. Meteor. Soc.*, **83**, 363–376, https://doi.org/10.1175/1520-0477-83.3.363.

Brown, T. M., D. Liang, and J. A. Womble, 2012: Predicting ground-based damage states from windstorms using remote-sensing imagery. *J. Wind Struct.*, **15**, 369–383, https://doi.org/10.12989/was.2012.15.5.369.

Camp, P. J., 2013a: Damage Assessment Toolkit training, part I. YouTube, www.youtube.com/watch?v=Kzi0cUqr9YQ.

——, 2013b: Damage Assessment Toolkit training, part II. YouTube, www.youtube.com/watch?v=71YVnbj5FQ4.

——, L. P. Rothfusz, A. Anderson, D. Speheger, K. L. Ortega, and B. R. Smith, 2014: Assessing the Moore, Oklahoma (2013) tornado using the National Weather Service Damage Assessment Toolkit. *Special Symp. on Severe Local Storms*, Atlanta, GA, Amer. Meteor. Soc., 830, https://ams.confex.com/ams/94Annual/webprogram/Paper233734.html.

Edwards, R., J. G. LaDue, J. T. Ferree, K. Scharfenberg, C. Maier, and W. L. Coulbourne, 2013: Tornado intensity estimation: Past, present, and future. *Bull. Amer. Meteor. Soc.*, **94**, 641–653, https://doi.org/10.1175/BAMS-D-11-00006.1.

Gallo, K., T. Smith, K. Jungbluth, and P. Schumacher, 2012: Hail swaths observed from satellite data and their relation to radar and surface-based observations: A case study from Iowa in 2009. *Wea. Forecasting*, **27**, 796–802, https://doi.org/10.1175/WAF-D-11-00118.1.

——, P. Schumacher, J. Boustead, and A. Ferguson, 2019: Validation of satellite observations of storm damage to cropland with digital photographs. *Wea. Forecasting*, **34**, 435–446, https://doi.org/10.1175/WAF-D-18-0059.1.

Giglio, L., T. Loboda, D. P. Roy, B. Quayle, and C. O. Justice, 2009: An active-fire based burned area mapping algorithm for the MODIS sensor. *Remote Sens. Environ.*, **113**, 408–420, https://doi.org/10.1016/j.rse.2008.10.006.

Jedlovec, G. J., 2013: Transitioning research satellite data to the operational weather community: The SPoRT paradigm. *IEEE Geosci. Remote Sens. Mag.*, **1**, 62–66, https://doi.org/10.1109/MGRS.2013.2244704.

——, U. Nair, and S. L. Haines, 2006: Detection of storm damage tracks with EOS data. *Wea. Forecasting*, **21**, 249–267, https://doi.org/10.1175/WAF923.1.

Kingfield, D. M., and K. M. de Beurs, 2017: Landsat identification of tornado damage by land cover and an evaluation of damage recovery in forests. *J. Appl. Meteor. Climatol.*, **56**, 965–987, https://doi.org/10.1175/JAMC-D-16-0228.1.

Klimowski, B. A., M. R. Hjelmfelt, M. J. Bunkers, D. Sedlacek, and L. R. Johnson, 1998: Hailstorm damage observed from the *GOES-8* satellite: The 5–6 July 1996 Butte–Meade storm. *Mon. Wea. Rev.*, **126**, 831–834, https://doi.org/10.1175/1520-0493(1998)126<0831:HDOFTG>2.0.CO;2.

Knupp, K. R., and Coauthors, 2014: Meteorological overview of the devastating 27 April 2011 tornado outbreak. *Bull. Amer. Meteor. Soc.*, **95**, 1041–1062, https://doi.org/10.1175/BAMS-D-11-00229.1.

Lakshmanan, V., T. Smith, G. Stumpf, and K. Hondl, 2007: The Warning Decision Support System–Integrated Information. *Wea. Forecasting*, **22**, 596–612, https://doi.org/10.1175/WAF1009.1.

Leonardo, D., 2011: Damage Assessment Toolkit business case analysis: NWS OSIP Project 08-024. NWS Rep., 16 pp., https://osip.nws.noaa.gov/osip/projectDetail.php?document=23295.

Molthan, A. L., G. J. Jedlovec, and B. Carcione, 2011: NASA satellite data assist in tornado damage assessments. *Eos, Trans. Amer. Geophys. Union*, **92**, 337–339, https://doi.org/10.1029/2011EO400002.

——, J. E. Burks, K. M. McGrath, and F. J. LaFontaine, 2013: Multi-sensor examination of hail damage swaths for near real-time applications and assessment. *J. Oper. Meteor.*, **1**, 144–156, https://doi.org/10.15191/nwajom.2013.0113.

——, J. R. Bell, T. A. Cole, and J. E. Burks, 2014: Satellite-based identification of tornado damage tracks from the 27 April 2011 severe weather outbreak. *J. Oper. Meteor.*, **2**, 191–208, https://doi.org/10.15191/nwajom.2014.0216.

Myint, S. W., M. Yuan, R. S. Cerveny, and C. P. Giri, 2008: Comparison of remote sensing image processing techniques to identify tornado damage areas from Landsat TM data. *Sensors*, **8**, 1128–1156, https://doi.org/10.3390/s8021128.

NASA SPoRT, 2019: Damage Assessment Toolkit quick guides. NASA, https://weather.msfc.nasa.gov/sport/disasters/dat/quickguides/.

National Wind Institute, 2006: A recommendation for an enhanced Fujita scale (EF-scale). Texas Tech University Wind Science and Engineering Center Rep., 111 pp., www.depts.ttu.edu/nwi/Pubs/EnhancedFujitaScale/EFScale.pdf.

NOAA, 2018: Post-storm data acquisition. National Weather Service Instruction 10-1604, 14 pp., www.nws.noaa.gov/directives/sym/pd01016004curr.pdf.

——, 2019a: NOAA/NWS Damage Assessment Toolkit course orientation. National Weather Service, https://training.weather.gov/wdtd/courses/EF-scale/DAT-course/Orientation/interaction_html5.html.

——, 2019b: Historic outbreak of April 27, 2011. National Weather Service, www.weather.gov/bmx/event_04272011.

——, 2019c: 2015 Iowa tornadoes. National Weather Service, www.weather.gov/dmx/iators2015.

——, 2019d: December 23, 2015 tornado outbreak. National Weather Service, www.weather.gov/ohx/20151223.

——, 2019e: 7th anniversary of the Joplin tornado of May 22, 2011. National Weather Service, www.weather.gov/sgf/news_events_2011may22.

——, 2019f: Deadly tornado outbreak of January 22, 2017. National Weather Service, www.weather.gov/tae/20170122_tornadoes.

Parker, M. D., I. C. Ratcliffe, and G. M. Henebry, 2005: The July 2003 Dakota hailswaths: Creation, characteristics, and possible impacts. *Mon. Wea. Rev.*, **133**, 1241–1260, https://doi.org/10.1175/MWR2914.1.

Pearson, W. L., and K. S. Lander, 2008: Server GIS: Lessons learned from an ESRI ArcServer demonstration project at the NWS Central Region Headquarters. *24th Conf. on IIPS*, New Orleans, LA, Amer. Meteor. Soc., 5A.11, https://ams.confex.com/ams/88Annual/techprogram/paper_132019.htm.

Rosen, P. A., and Coauthors, 2015: The NASA-ISRO SAR mission: An international space partnership for science and societal benefit. *2015 Radar Conf.*, Arlington, VA, IEEE, 1610–1613, https://doi.org/10.1109/RADAR.2015.7131255.

Schultz, L. A., 2017: Detecting tornado tracks using synthetic aperture radar (SAR) imagery. WordPress, https://nasasport.wordpress.com/2017/06/05/detecting-tornado-tracks-using-synthetic-aperture-radar-sar-imagery.

Shamburger, S., 2016: Landsat DAT imagery helps determine tornado tracks. WordPress, https://nasasport.wordpress.com/2016/04/11/landsat-dat-imagery-helps-determine-tornado-tracks/.

Skow, K. D., and C. Cogil, 2016: A high-resolution aerial survey and radar analysis of quasi-linear convective system surface vortex damage paths from 31 August 2014. *Wea. Forecasting*, **32**, 441–467, https://doi.org/10.1175/WAF-D-16-0136.1.

Stellman, K., T. Brice, D. Hansing, A. Foster, C. Pieper, and K. Lander, 2009: How geographic information system software is improving the effectiveness of the National Weather Service. *89th Annual Meeting*, New Orleans, LA, Amer. Meteor. Soc., 5A.11, http://ams.confex.com/ams/89annual/webprogram/Paper148642.html.

Stumpf, G. J., T. M. Smith, and J. Hocker, 2004: New hail diagnostic parameters derived by integrating multiple radars and multiple sensors. *22nd Conf. on Severe Local Storms*, Hyannis, MA, Amer. Meteor. Soc., P7.8, http://ams.confex.com/ams/pdfpapers/81451.pdf.

Sun, D., S. Li, R. Zhang, and Y. Yu, 2012: Towards operational automatic flood detection using EOS/MODIS data. *Photogramm. Eng. Remote Sensing*, **78**, 637–646, https://doi.org/10.14358/PERS.78.6.637.

Tucker, C. J., 1979: Red and photographic infrared linear combinations for monitoring vegetation. *Remote Sens. Environ.*, **8**, 127–150, https://doi.org/10.1016/0034-4257(79)90013-0.

Witt, A., M. D. Eilts, G. J. Stumpf, J. T. Johnson, E. D. Mitchell, and K. W. Thomas, 1998: An enhanced hail detection algorithm for the WSR-88D. *Wea. Forecasting*, **13**, 286–303, https://doi.org/10.1175/1520-0434(1998)013<0286:AEHDAF>2.0.CO;2.

Womble, J. A., R. L. Wood, and M. E. Mohammadi, 2018: Multi-scale remote sensing of tornado effects. *Front. Built Environ.*, **4**, 66, https://doi.org/10.3389/fbuil.2018.00066.

Yuan, M., M. Dickens-Micozzi, and M. A. Magsig, 2002: Analysis of tornado damage tracks from the 3 May tornado outbreak using multispectral satellite imagery. *Wea. Forecasting*, **17**, 382–398, https://doi.org/10.1175/1520-0434(2002)017<0382:AOTDTF>2.0.CO;2.